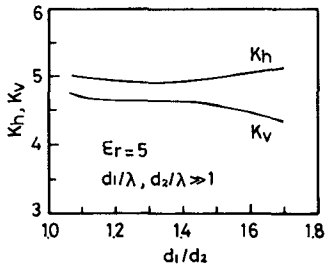

Fig. 11. Numerical coefficient versus aspect ratio of the arched tunnel.

and K_v are calculated in Fig. 11 as a function of aspect ratio d_1/d_2.

VI. Conclusion

We have presented the attenuation constants of the dominant modes corresponding to horizontal and vertical polarizations of the electric field in arched tunnels based on the point-matching method combined with Muller's method. The calculated values agree well with experimental results, and the validity of the previous experimental equation is confirmed theoretically for the horizontally polarized mode. Then, due to the fact that the difference in the attenuation constant between rectangular and circular tunnels is expressed only by a numerical coefficient in the approximate equations, we derived a similar equation for arched tunnels based on the point-matching solution considering polarization characteristics. The resultant equation can be used directly to determine or estimate the value for UHF radio frequencies.

Acknowledgment

The authors would like to thank Profs. N. Goto, Y. Naito, Y. Simizu, and T. Iijima, Faculty of Engineering, Tokyo Institute of Technology, for many helpful discussions and suggestions.

References

[1] J. Chiba, T. Inaba, Y. Kuwamoto, O. Banno, and R. Sato, "Radio communication in tunnels," *IEEE Trans. Microwave Theory Tech.*, vol. MTT-26, pp. 439–443, June 1978.

[2] T Inaba, Y. Kuwamoto, O. Banno, J. Chiba, and R. Sato, "Approximate solution of the attenuation constant of cylindrical tunnels," *Trans. IECE of Japan*, vol. J62-B, no. 4, pp. 435–436, Apr. 1979 (in Japanese).

[3] Y. Yamaguchi and T. Sekiguchi, "Propagation characteristics of normal modes in hollow circular cylinder surrounded by dissipative medium," *Trans. IECE of Japan*, vol. J62-B, no. 4, pp. 368–373, Apr. 1979 (in Japanese).

[4] A. G. Emslie, L. L. Robert, and P. F. Strong, "Theory of the propagation of UHF radio waves in coal mine tunnels," *IEEE Trans. Antennas Propagat.*, vol. AP-23, pp. 192–205, Mar. 1975.

[5] S. F. Mahmoud and J. R. Wait, "Geometrical optical approach for electromagnetic wave propagation in rectangular mine tunnels," *Radio Sci.*, vol. 9, no. 12, pp. 1147–1158, 1974.

[6] Y. Yamaguchi, T. Shimizu, and T Abe, "Propagation characteristics of the dominant mode in tunnels with elliptical cross section," *Trans. IECE of Japan*, vol. J64-B, no. 9, pp. 1032–1038, Sept. 1981 (in Japanese).

[7] J. Chiba, "Studies of helix," M.S. thesis, Faculty Eng., Tohoku Univ., Japan, pp. 32–185, 1957.

[8] J. Chiba, T. Inaba, Y. Kuwamoto, O. Banno, and R. Sato," Attenuation constants and phase constants of the tunnels," *Trans. 1987 ISAP Japan*, C-3-4, pp. 389–392, Aug. 1987.

[9] Y. Yamaguchi, T. Abe, and T. Sekiguchi, "Propagation characteristics of the dominant mode in tunnels," *Trans. IECE of Japan*, vol. J65-B, no. 4, pp. 471–476, Apr. 1982 (in Japanese).

[10] J. E. Goell, "A circular-harmonic computer analysis of rectangular dielectric waveguides," *Bell Syst. Tech. J.*, vol. 48, pp. 2133–2160, Sept. 1969.

[11] S D. Conte and C. de. Boor, *Elementary Numerical Analysis*, 3rd ed. New York: McGraw-Hill, 1981, ch. 3, pp. 120–125.

[12] E. A. J. Marcatili and R. A. Schmeltzer, "Hollow metallic and dielectric waveguides for long distance optical transmission and lasers," *Bell Syst. Tech. J.*, vol. 43, pp. 1783–1809, July 1964.

The Thermal and Spatial Resolution of a Broad-Band Correlation Radiometer with Application to Medical Microwave Thermography

JOSEPH C. HILL, MEMBER, IEEE, AND
RONALD B. GOLDNER, SENIOR MEMBER, IEEE

***Abstract*—The improved spatial and thermal resolution of a broad-band microwave correlation radiometer is discussed. Theoretical upper and lower bounds of the combined spatial and thermal resolution in a dense transmission medium are presented along with data obtained for two thermal sources in air. The application of broad-band correlation techniques to medical microwave thermography is novel, and the results indicate that electronic scanning of tissue should be possible.**

I. Introduction

Coherence theory [1] and its application to correlation radiometery [2], [3] has been discussed extensively in the literature and has been employed in radio astronomy for over 30 years. Because of its improved spatial resolution, correlation radiometry has received considerable interest in its application to medical microwave thermography [4]–[7].

Previous publications [4] have discussed a correlator employing a "pencil beam" antenna pattern formed by beam multiplication of partially overlapping antenna patterns, such as shown in Fig. 1(a), which permits examination of a small volume of tissue. However, examining an adjacent volume of tissue would require that the antennas be physically moved relative to the patient.

Recent publications [5], [6] have discussed measurements employing overlapping antenna beams as shown in Fig. 1(b). The enclosed volume of tissue, which is larger than that viewed by the "pencil beam" antenna pattern, should be able to be scanned electronically by introducing a delay in one arm of the correlator with the antennas stationary. Electronic scanning utilizing the radiometer delay [7] is distinct from aperture synthesis radiometery [8], in which the longitudinal coherence function, or mutual intensity function, is measured at several different locations by either antenna movement or antenna switching, with the radiometer delay set to zero [3]. Image reconstruction using aperture synthesis techniques is the microwave analogue of a van Cittert–Zernike experiment[1] in optics.

In this paper, we discuss the cross correlation of thermal radiation from two sources received by two antennas that are at a

Manuscript received October 15, 1984; revised March 18, 1985. This work was supported in part by a Tufts University biomedical research grant, HEW 1-SO7-RR07179-01 [7].

J. C. Hill is with Enon Microwave Inc, Topsfield, MA 01983.

R. B. Goldner is with the Department of Electrical Engineering, Tufts University, Medford, MA 02155.

[1]The van Cittert–Zernike theorem states that if the delay in the two paths of the correlator is much less than the reciprocal of the bandwidth, then the mutual intensity function, as measured across the detection plane, is equal to the Fourier transform of the brightness of the source distribution [1].

0018-9480/85/0800-0718$01.00 ©1985 IEEE

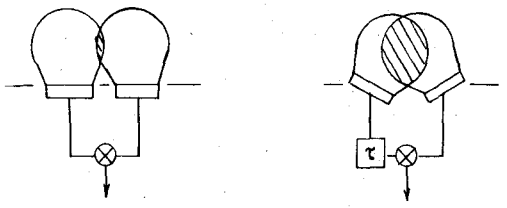

Fig. 1. Comparison of antenna patterns. (a) Pencil beam. (b) Overlapping beam.

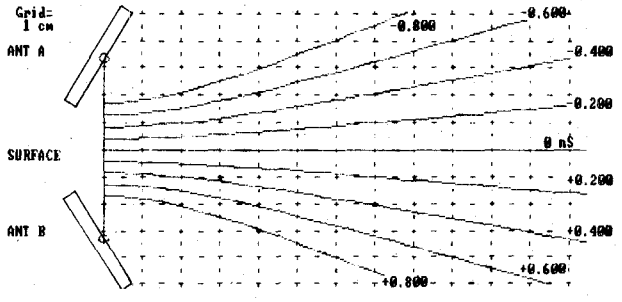

Fig. 2. Curves of constant delay difference for a dielectric constant = 49.

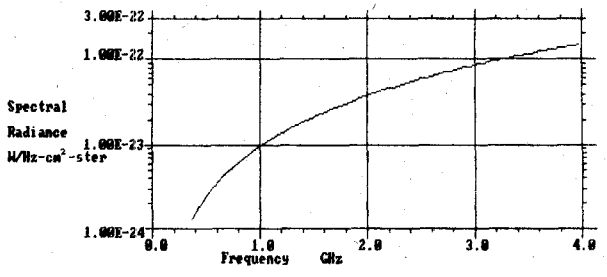

Fig. 3. Thermal radiation of a black body at 37°C in the frequency range of 0–4 GHz.

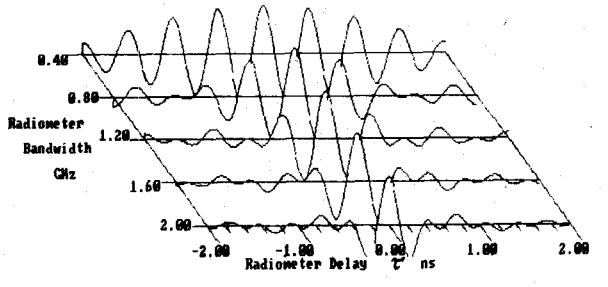

Fig. 4. Correlation of a single source versus bandwidth for $F_c = 2.0$ GHz and $\tau = 0$.

fixed distance to the sources and to one another. Since the application of broad-band correlation techniques to medical microwave thermography is novel, new concepts are presented. These are the surfaces of constant delay and the apparent coherence time of the radiation. We also discuss the implications that broad-band correlation should have on the spatial and thermal resolution of such measurements performed in dense tissue. Preliminary data of two thermal sources in air is presented. From this data, lower and upper limits of combined spatial and thermal resolution are calculated for thermal sources in dense tissue.

II. Discussion

A two-antenna microwave correlation radiometer integrates radiation over a surface that is of a fixed time delay difference to the two antennas and also is within the volume of tissue common to both antennas. This surface is defined such that the difference in transit time of the radiation from any point P on that surface to each of the antennas is a constant τ'. If $X1$ and $X2$ are the vectors from P to each antenna and c is the speed of light in the tissue, then $\tau' = x/c$, where $x = |X1| - |X2|$. Although a two-antenna radiometer cannot distinguish radiation from different points on a surface of constant delay, the radiometer can distinguish radiation from surfaces of different constant delay. The ability to resolve these surfaces depends on the apparent coherence time of the radiation which, as will be shown, is determined by the receiver bandwidth.

Lines of constant delay for a typical experiment are shown in Fig. 2. Both antennas of the correlator, separated by 6.5 cm, are mounted on the surface of the tissue. The lines of constant delay are formed at the intersection of the surfaces of constant delay and the plane of the antennas. A dielectric constant of 49 was chosen since it is typical of dense tissue [9]. A grid of 1-cm intervals is overlayed on the lines of constant delay; as will be discussed below, this grid will be used to assist in determining the spatial resolution from the calculated delay resolution. This simple model assumes propagation in a lossless, homogeneous medium with noninteracting antennas of negligible size.

The microwave correlation process can be described as the cross correlation of two stationary (wide sense), ergodic random variables

$$C\{t\} = \langle V_a(t) V_b^*(t-\tau) \rangle = V_a(f,t,\theta) V_b^*(f,t-t,\theta)\, p(f,t,\theta)\, df dt d\theta \quad (1)$$

where V_a is the voltage at antenna A, V_b the voltage at antenna B, and p the probability distribution of the radiation over frequency, time, and phase. The frequency distribution of black-body radiation is described by Planck's law. The microwave radiometer, however, selects only a small portion of the entire spectrum emitted by a black body. The total radiation emitted by a black body at 310°K is plotted over the frequency of interest in Fig. 3. In this paper, we assume a uniform probability distribution over frequency. This uniform distribution can be accomplished by appropriately compensating the gain characteristics of the radiometer over frequency to complement the curve of Fig. 3; this must be done without compromising the noise figure of the radiometer.

With the simplifying assumption of uniform frequency distribution and of random phase, the integration of (1) is straightforward. The normalized correlation of a point source as a function of the spatial delay and the radiometer delay is

$$C\{\tau' - \tau\} = \cos(\pi(f2+f1)(\tau' - \tau)) \cdot \operatorname{sinc}(\pi(f2-f1)(\tau' - \tau)) \quad (2)$$

where $f2$ is the upper frequency, $f1$ is the lower frequency, τ' is the spatial time delay, τ is the radiometer time delay.

This function is plotted in Fig. 4 for a source located on the surface of delay $\tau' = 0$ as a function of radiometer delay (τ) and bandwidth ($f2 - f1$) for a center frequency of 2.00 GHz. This frequency range was selected because the attenuation in living tissue is considerably less near 2 GHz as compared to the attenuation at higher frequencies. Also, such a microwave radiometer can be easily constructed using commercially available broad-band components, such as low-noise preamplifiers and mixers.

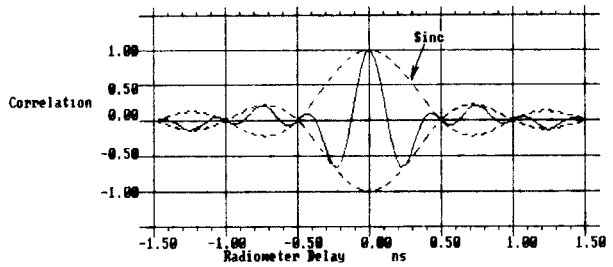

Fig. 5. Correlation of a point source located at $\tau = 0$ showing the sinc envelope; radiometer bandwidth: 1–3 GHz.

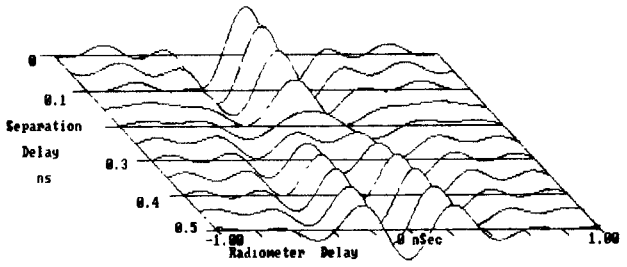

Fig. 6. Calculated correlation of two sources centered at $\tau = 0$ with variable spacing; radiometer bandwidth: 1–3 GHz.

The coherence time of radiation is commonly defined [1, secs. 7.58 and 10.1] as being on the order of the reciprocal of the bandwidth of the radiation. If we use the conventional 3-dB definition for bandwidth, then the bandwidth of the radiation is approximately 10^{13} Hz, calculated using Plank's law [10] for a black body at 310°K. However, the portion of the electromagnetic spectrum that is sampled by the microwave radiometer is at most 10^{10} Hz. For this reason, we refer to the coherence time measured by the microwave radiometer as the "apparent" coherence time. We define the apparent coherence time τ_0 as being that time for which the sinc envelope of (1) is one half its value at zero delay.

From Figs. 4 and 5, we see that as the bandwidth increases from 0.40 to 2.00 GHz, the apparent coherence time decreases from $+/-1.50$ ns to $+/-0.30$ ns. For total transit time differences $(\tau' - \tau)$ greater than τ_0, the radiation will decorrelate. Thus, depending on the setting of the radiometer delay τ, one can examine successive volumes of tissue that are bounded by surfaces of constant delay $\tau' + \tau_0$ and $\tau' - \tau_0$, where $\tau' = \tau$. Born and Wolf refer to this as the region of coherence [1]. In addition to the angular beamwidth of the individual antennas, we may now describe a correlation radiometer by its coherence or delay beamwidth. If we examine Fig. 2, we see that at 3 cm below the surface of the medium under discussion, the apparent coherence time of $\tau_0 = +/-0.30$ ns for a radiometer bandwidth from 1.0 to 3.0 GHz corresponds to a coherence beamwidth of approximately $+/-0.9$ cm.

We may now discuss the limits of thermal and spatial resolution of a broad-band correlation radiometer. The upper limit can be estimated by considering the correlation of two sources of the same temperature on various surfaces of constant delay. If we assume that the sources are uncorrelated and are in a reflection-free medium, then the total correlation pattern is the sum of the individual correlation patterns. The output of the radiometer is plotted in Fig. 6 for different source delay spacings τ_s, as a function of the radiometer delay τ. As can be seen, there are two distinct patterns for source spacings greater than approximately 0.25 ns. Below this spacing, the traces merge and it is not possible

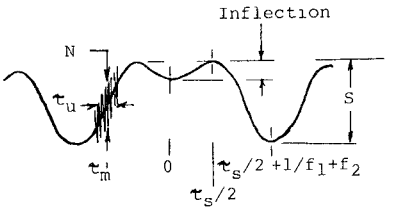

Fig. 7. Theoretical correlation of two sources separated by 0.25 ns with associated measurement errors.

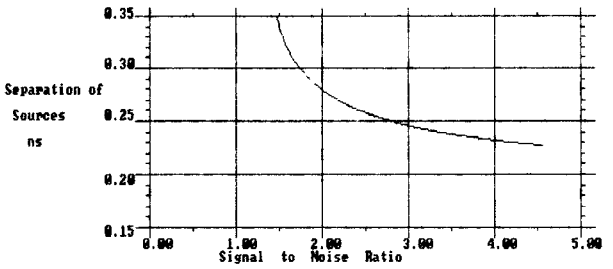

Fig. 8. Minimum resolvable separation of two sources at the same temperature as a function of signal-to-noise ratio; radiometer bandwidth: 1–3 GHz

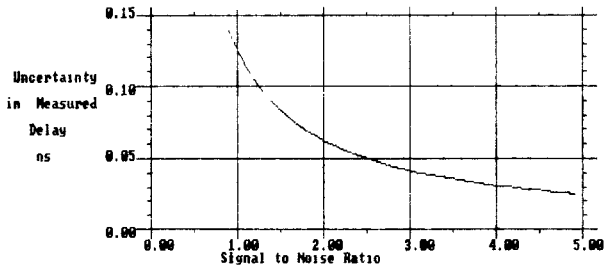

Fig. 9. Uncertainty in the measured delay as a function of the signal-to-noise ratio; radiometer bandwidth: 1–3 GHz.

to distinguish the individual patterns without further processing. As the signal-to-noise ratio (S/N) decreases, the spacing at which the sources are distinct must increase.

Fig. 7 is the calculated output of the radiometer for two sources separated by a delay of 0.25 ns. If we set the inflection in the correlation equal to the noise, then from Fig. 7 the minimum separation of the two sources is related to the signal-to-noise ratio as follows:

$$S/N = \left[C\{\tau_s/2\} - C\{\tau_s/2 + 1/(f1+f2)\}\right] / \left[C\{\tau_s/2\} - C\{0\}\right]. \quad (3)$$

This function defines the upper limit of the combined spatial and thermal resolution; τ_s' is plotted as a function of the signal-to-noise ratio in Fig. 8. The normalized signal-to-noise ratio is used as the independent variable instead of the absolute temperature of the source since the two-antenna correlation radiometer cannot distinguish between a weak signal close to the antennas and a stronger signal (i.e., hotter source) on the same surface of delay farther away in a lossy medium.

To improve the spatial resolution, further processing is required to recover the original thermal distribution. The resolution of such a process is limited by the uncertainty in the measured delay as a function of the signal-to-noise ratio. From Fig. 7, the uncertainty can be estimated from the noise on the signal at the point of maximum slope of the correlation function. This uncer-

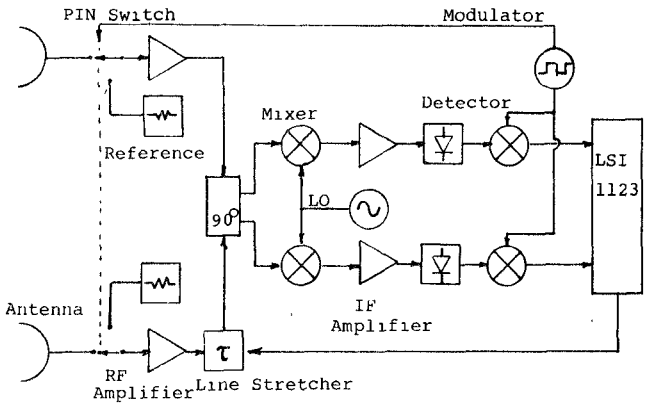

Fig. 10. Schematic representation of the dual IF correlation radiometer.

TABLE I
RADIOMETER SPECIFICATIONS

RF Amplifier Noise Figure:	3.5	dB
Minimum Resolution (measured):	0.04	°K
Frequency RF:	2.6–3.4	GHz
IF:	10–400	MHz
Delay Total:	2.17	nS
Number of Bits:	7	
Increments:	0.017	nS
Modulating Frequency:	5.0	KHz
Duty Ratio:	0.5	
Integration Time:	3.0	s
Antenna Aperture:	1.34×2.84	in
	(3.40×7.21)	cm
Antenna Spacing (on center):	3.0	in
	(7.62)	cm

tainty is

$$\tau_u = 1/[\mathrm{S/N}\, dC\{\tau\}/d\tau] \qquad (4)$$

where the derivative is evaluated at τ_m, the zero crossing point of the correlation function. This function, which represents the lower limit in spatial and thermal resolution, is plotted in Fig. 9.

III. EXPERIMENTS

An experiment was designed to examine the surfaces of constant delay in air using two thermal sources. A previously described stabilized correlation radiometer [5] was used with the gain appropriately compensated for the black-body radiation over the operating bandwidth of 2.6 to 3.4 GHz. A schematic representation of the radiometer is shown in Fig. 10. Before each RF amplifier was a p-i-n diode switch to modulate the RF. The delay was introduced in one of the RF channels by means of a seven-bit digital line stretcher, which was under the control of a DEC LSI 11/23 computer. The signals from each RF channel were combined by means of a quadrature hybrid and then down converted to two IF signals. The difference of the outputs of the synchronous detectors was stored in the computer. Long term drifts, such as antenna-source match and background temperature change, were minimized by taking the difference of the IF signals. The radiometer performance is summarized in Table I.

Two resistively heated thermal sources, separated by 1.3 cm, were mounted approximately 5 cm from each of the antennas as shown in Fig. 11. The lines of constant delay in the plane of the antennas, whose centerlines were spaced at 7.5 cm in air, are shown in Fig. 11. From the calibration grid of 1-cm spacing that

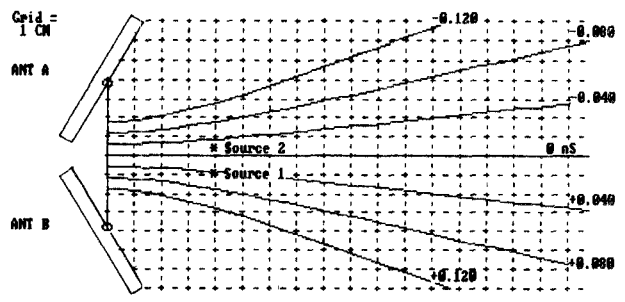

Fig. 11. Curves of constant delay difference for dielectric constant = 1.

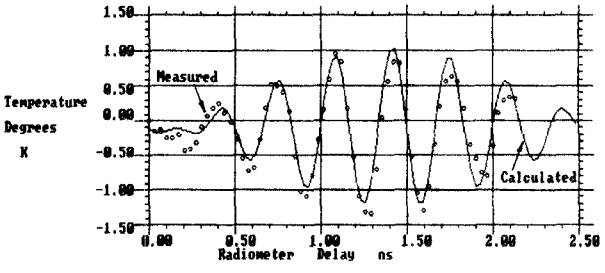

Fig. 12. Comparison of the correlation of a 1.15°K coaxial reference with the calculated correlation of a point source; radiometer bandwidth: 2.6–3.4 GHz.

is superimposed on the lines of constant delay, we see that this spatial separation corresponds to a delay separation of 0.06 ns. The sources were 0.64 cm wide and 5.0 cm long, oriented so that the long dimension was parallel to the E-field of the TE_{10} waveguide mode of the WR-287 open waveguide antennas and along a line of constant delay. The thermal sources were fabricated from carbon impregnated cloth of 400 Ω per square and were made one-half wavelength long at 3.0 GHz to insure reasonable radiation characteristics over the 2.6–3.4-GHz frequency band.

The radiometer was calibrated by measuring the correlation of a 1.15°K coaxial noise source simultaneously connected to both inputs of the correlator. The difference in correlation for the noise source on and off, which was stored in the computer and then digitally filtered, is shown in Fig. 12 along with the correlation calculated from (2). A total of 256 data points (128 in each state) were recorded with an integration time of 3 s. The calibration signal was turned off during the experiments.

Subtraction was used to eliminate previously discussed background correlation terms [5], due to contributions such as the mutual illumination of the antennas. This measurement technique is consistant with hyperthermia treatment, in which the correlation is measured before and after the application of heat. The subtraction does pose a problem for volume thermographic imaging; it is anticipated that this will be overcome in the future.

The minimum source temperature change that the system was capable of resolving was measured in the following way. The change in the output of the radiometer was recorded as source 1 was heated to several temperatures above room temperature (2.3, 4.5, 6.7, and 9°C). As before, the difference in the correlation of the thermal source off (room temperature) and then on (elevated temperature) was recorded and digitally filtered. The temperature measured by the radiometer is plotted as a function of the source temperature in Fig. 13. In these experiments, the minimum temperature that the radiometer could resolve was 0.04°C. This number includes errors associated with line stretcher variations during the 20 min of the experiment. Using 0.04°C as the

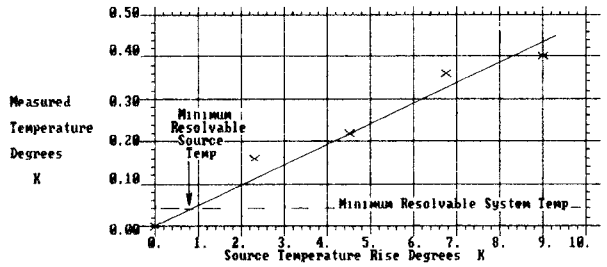

Fig. 13. Comparison of the source temperature with the measured temperature for calculation of the minimum resolvable source temperature.

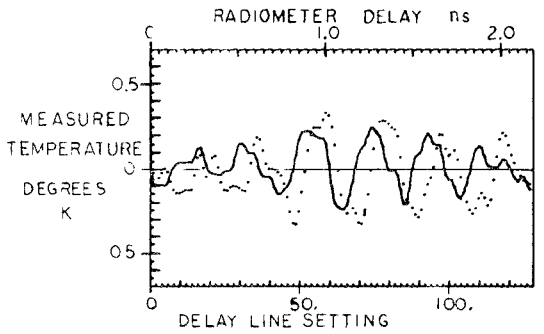

Fig. 14. Correlation of two sources in air separated by 1 3 cm

minimum resolvable system temperature, extrapolation of the data points of Fig. 13 show that a signal-to-noise ratio of unity would be measured for a source temperature of 0.8°C. This was defined as the minimum resolvable source temperature of the radiometer.

Source 1 was heated to 4.5°C above ambient and its correlation is shown in Fig. 14. The correlation is plotted as a function of the radiometer delay as well as the setting of the 7-bit digital line stretcher. When the source was moved toward the antennas along a line of constant delay, there was no perceptible change in the delay of the correlation pattern. When source 2 was heated to 4.5°C above ambient, with source 1 off, the correlation pattern shifted approximately 0.07 ns, as shown in Fig. 14. This is in reasonable agreement with the numbers predicted by the simplified model of Fig. 11. Both sources were turned on together, and, as expected, the measured correlation was the linear sum of the individual patterns.

IV. Limits of Resolution

We may now calculate the upper and lower bounds of the combined spatial and thermal resolution that can be obtained in measuring thermal sources. We will assume that the correlating radiometer has a bandwidth from 1.0 to 3.0 GHz. One important application of such a radiometer is the passive monitoring of the temperature of breast tumors. It has been described in the literature that cancerous tumors of the breast are hotter than the surrounding normal tissue [11] by at least 1°C.

In the last section, a S/N ratio of unity was obtained with a source temperature of 0.8°C, measured with a radiometer bandwidth of 0.8 GHz. Since the thermal resolution varies as the square root of the bandwidth, increasing the radiometer bandwidth from 0.8 GHz to 2.0 GHz will improve the thermal resolution such that a source temperature change of 0.50°C will have a S/N ratio of unity.

A 1.0°C source with a 0.50°C noise level will yield a signal-to-noise ratio of 2.0:1. The upper limit of delay resolution for this S/N ratio from Fig. 8 is 0.28 ns; the lower limit from Fig. 9 is 0.06 ns. If we assume that sources of the same cross-sectional area are immersed in a dense medium of dielectric constant 49 and positioned 3 cm from the surface, then from the plots of constant delay of Fig. 2, this range of delay resolution corresponds to a range of spatial resolution between 2.0 mm and 9.3 mm.

V. Conclusions

The concept of surfaces of constant delay was presented. It has been shown that, as the receiver bandwidth increased, the apparent coherence time of the radiation decreased, permitting a narrow volume of tissue to be examined. Consequently, this means that the volume of tissue under examination can be scanned electronically as a function of the delay setting of the radiometer. Based upon preliminary experiments in air with the current equipment, a spatial resolution of between 2.0 and 9.3 mm should be achievable for a source 1°C above the surrounding tissue.

Based upon the model discussed in this paper, together with additional experiments, we believe that a broad-band correlation radiometer will permit a more accurate thermal measurement during hyperthermia treatment and could lead to volume thermographic imaging. That is, the limiting factor for the spatial and thermal resolution is the noise level of the radiometer currently being used. As the sensitivity of the radiometer system improves, the spatial resolution will also improve. We feel that these numbers are very encouraging and justify continued work to address the more practical problems associated with propagation in an inhomogeneous, lossy medium, and measurement with antennas of finite size.

References

[1] M. Born and E. Wolf, *Principle of Optics*. London: Pergamon Press, 1965, ch. 10.
[2] H. C. Ko, "Coherence theory of radio astronomical measurements," *IEEE Trans. Antennas Propagat.*, vol. AP-15, pp. 10–17, Jan. 1967.
[3] G. Swenson and N. Mathur, "The interferometer in radio astronomy," *Proc. IEEE*, vol. 56, pp. 2114–2130, Dec. 1968.
[4] A. Mamouni, Y. Leroy, J. C. Van DeVelde, and L. Bellarbi, "Correlation microwave thermography," in *Proc. 12th Eur. Conf.* (Helsinki), Sept. 1982, pp. 553–558.
[5] J. C. Hill and R. B. Goldner, "A stabilized broadband correlator for medical microwave thermography," in *Proc. 1984 IEEE MTT-S Int. Symp.* (San Francisco, CA), May 30–June 1, 1984, pp. 368–370.
[6] L. Bellari, A. Mamouni, J. C. Van DeVelde, and Y. Leroy, "Gradients in lossy materials by correlation microwave thermography," *Electron. Lett.*, vol. 20, pp. 430–431, May 1984.
[7] Final report, Tufts University Research Committee, HEW Grant No. 1-SO7-RR07179-0, 1978–1979. This brief report is available directly from the Electrical Engineering Department, Tufts University, Medford, MA 02155.
[8] N. C. Haslam, A. R. Gillespie, and C. G. T. Haslam, "Aperture synthesis thermography—A new approach to passive microwave temperature measurements in the body," *IEEE Trans. Microwave Theory Tech.*, vol. MTT-32, pp. 829–835, Aug. 1984.
[9] C. C. Johnson and A. W. Guy, "Nonionizing electromagnetic wave effects in biological materials and systems," *Proc. IEEE*, vol. 60, pp. 692–718, June 1972.
[10] Harvey, *Microwave Engineering*. London: Academic Press, 1963, sec. 16.4.
[11] R. N. Lawson and M. S. Chugtai, "Breast cancer and body temperature," *Canad. Med. Assn.*, vol. J88, pp. 68–70, Jan. 1963.